DIVIMP-B2-EIRENE modelling of ^{13}C migration and deposition in ASDEX Upgrade L-mode plasmas

A Xuereb[a,b1], M Groth[a2], K Krieger[c], O Asunta[a], T Kurki-Suonio[a],
J Likonen[d], D P Coster[c] and the ASDEX Upgrade Team

[a] *Association Euratom-Tekes, Helsinki University of Technology, P.O.Box 4100, FI-02015 TKK, Finland*

[b] *School of Physics and Astronomy, University of Southampton, Southampton SO17 1BJ, United Kingdom*

[c] *Max-Planck-Institut für Plasmaphysik, Euratom Association, Boltzmannstr. 2, D-85748 Garching, Germany*

[d] *Association Euratom-Tekes, VTT, P.O.Box 1000, FI-02044 VTT, Finland*

Abstract

Carbon transport and migration were studied experimentally and numerically in a high-density, low-confinement mode plasma in the ASDEX Upgrade tokamak. On the last day of plasma operation of the 2004-2005 experimental campaign, ^{13}CH$_4$ was injected into the vacuum vessel from the low field side midplane. A poloidal set of tiles was subsequently removed and analysed for ^{13}C deposition. In this work the measured deposition profile is interpreted using the impurity transport code DIVIMP. The simulated poloidal distribution of ^{13}C deviates significantly from the measured profile. The simulations indicate that ^{13}C is promptly deposited at the wall in the vicinity of the injection port, and is transported to the low field side divertor plate predominately via the scrape-off layer. The B2-EIRENE plasma solution produce stagnant plasma flow in the main scrape-off layer, in contrast to measurements in ASDEX Upgrade and other tokamaks. This is the likely cause of

---

[1]This work was carried out while A. Xuereb was performing a traineeship at the Advanced Energy Systems laboratory of the Helsinki University of Technology (Espoo, Finland).

[2]Corresponding author. Telephone: +358 9 451 3207, Fax: +358 9 451 3195, E-mail: mathias.groth@tkk.fi.

the discrepancy between the measured and the calculated poloidal distribution of the ^{13}C deposition. Key model parameters of DIVIMP were varied to determine their effect on the simulated deposition profile.

1. Introduction

One of the major challenges in future, fusion-relevant devices, such as ITER [1], is retention of radioactive tritium in in-vessel components. Because of tritium co-deposition with carbon, this issue is amplified in devices with carbon-based plasma facing components, which are currently foreseen to be used for the divertor target plates in ITER [2]. Understanding of the physics processes responsible for material migration and re-deposition of carbon in tokamak edge plasmas is thus of crucial importance for operation of future fusion devices.

The interpretation of campaign-integrated carbon migration studies is restricted because an experimental campaign generally consists of plasma discharges with many different configurations and confinement modes, all of which can exhibit very different impurity dynamics. Therefore, only limited phenomenological information about carbon dynamics can be derived from post-campaign analysis of retrieved wall components. Trace element studies provide a means to avoid this issue: a known amount of a trace element is injected into a series of identical plasma discharges, so that the trace impurity transport is solely due to one specific mode of operation. The spatial distribution re-deposited trace element can subsequently be quantified *ex-situ* at surfaces of tiles removed from the vessel. In this way, quantitative information about carbon migration and deposition for such a scenario can be obtained. Such experiments have been carried out in JET [3], ASDEX Upgrade (AUG) [4], and DIII-D [5], using ^{13}C as the isotopically tagged element. However, the deposition measurements by themselves cannot reveal the physics mechanisms responsible for the carbon migration. Numerical simulations of carbon dynamics in the scrape-off layer (SOL) and core regions are carried out to identify the most important physics behind carbon migration, and the corresponding tritium retention. These analyses include interpretative simulations with Monte Carlo-based impurity transport codes,

such as ERO [6] and DIVIMP [7].

The DIVIMP code has been extensively used to interpret ^{13}C injection experiments in DIII-D [8, 9, 10]. The DIII-D studies identified several physics processes as main contributors to the measured ^{13}C deposition observed at the high field side (HFS) divertor plate: plasma flow from the low field side (LFS) midplane toward the HFS divertor region, enhanced radial transport of carbon toward the HFS separatrix, and ^{13}C re-erosion/re-deposition at the HFS target.

In 2005, ^{13}CH$_4$ was injected into the AUG vessel during a sequence of identical L-mode discharges (Fig. 1(a)). A poloidal set of tiles was subsequently retrieved from the vessel and analysed for ^{13}C deposition [11]. The work presented in this paper aims at explaining the observed deposition profiles by DIVIMP impurity transport simulations coupled to a plasma background solution generated by the B2-EIRENE code as the principal input to DIVIMP. DIVIMP was used to calculate ^{13}C transport in the divertor and main SOL regions as well as in the pedestal region inside the separatrix, and to calculate the resulting ^{13}C deposition along the main chamber and divertor walls. Comparison with the measured ^{13}C deposition contributes to the benchmarking of predictive simulations of carbon transport and deposition for ITER with edge fluid codes.

The structure of this paper is as follows: the setup of DIVIMP and the input parameter and data are described in Sec. 2. A brief review of the experimental results is given in Sec. 3, followed by a comparison of the simulation results with the experimental data (Sec. 4). Finally, the results are summarised and discussed in Sec. 5.

2. General setup of DIVIMP simulations

The DIVertor IMPurity (DIVIMP) code [7] models impurity transport in the edge plasma region of tokamak fusion devices. It is a Monte Carlo code that follows impurity atoms and ion guiding centers along and across the magnetic field lines on a background plasma either prescribed using DIVIMP's internal plasma solvers or taken from other edge codes [12]. Parallel to the magnetic field lines the motion of the ions is computed based on classical transport, whereas perpendicular to the field lines, anomalous cross-field diffusion and convection are used [13]. The particle motion is traced on a 2D grid based on the measured magnetic equilibrium of a given discharge, Fig. 1(b). Although particle motion is followed along the helical field lines,
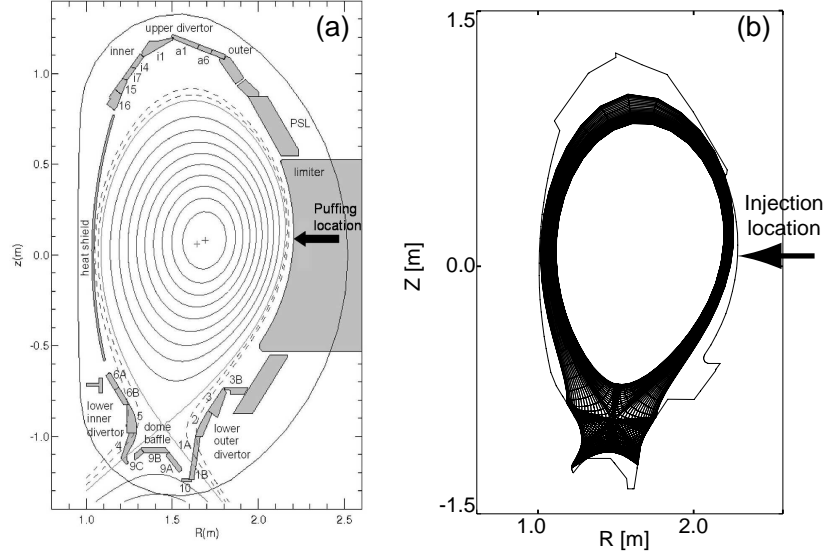
3

Figure 1: (a) Poloidal cross-section of ASDEX Upgrade vacuum vessel including tile numbers and the magnetic surfaces of AUG discharge #24046 at $t = 3.0$ s. (b) Two-dimensional grid based on the magnetic reconstruction of AUG discharge #17385 at $t = 2.4$ s. Several tiles are labeled for reference. (b) Poloidal cross-section of ASDEX Upgrade showing the measurement points used in the simulations.

all physical quantities are projected to the 2D grid representation in the poloidal plane assuming axisymmetry. Present fluid codes require grids, in which open field lines are limited by the target plates only, and thus the grid does generally not extend to the actual main chamber wall. DIVIMP allows, however, the recording of particle interaction with the actual divertor and main chamber wall outside the grid. The vessel wall structure used in the simulations is given by the poloidal cut of the ASDEX Upgrade vacuum vessel (Fig. 2). It should be noted that parts of the so defined surface correspond to non-axisymmetric structures, such as the ICRF antenna limiters at the LFS midplane. This has to be taken into account when interpreting the fluxes to and from these components.

In this work, a background plasma from a separate B2-EIRENE [14, 15] simulation was used with plasma parameters similar to those of the $^{13}CH_4$ injection experiment. The plasma configuration of the B2-EIRENE simulation, taken from AUG discharge #17385, differs from that of the ^{13}C injection experiment only by the vertical location of the strike points, which were lo-
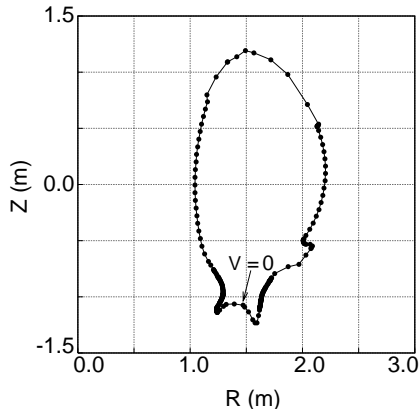
4

Figure 2: Coordinates of the vessel first wall vertices used for accounting of deposition in the DIVIMP simulations.

cated 2 cm lower in the $^{13}CH_4$ injection case. The background plasma was computed as a self-consistent solution of the coupled fluid equations for electrons, and fuel and carbon impurity ions. Closure of particle balance was resolved by coupling B2 iteratively to EIRENE for calculation of the fuel recycling and the intrinsic carbon source distribution. The carbon source was computed by EIRENE assuming physical and chemical sputtering of carbon by deuterium atoms and ions at the target plate. Match of the simulation and experimental electron density and temperature profiles at the upstream LFS midplane and divertor was obtained by varying the radial particle and heat transport coefficients. The simulation adequately describes the high-recycling plasma conditions observed in the LFS divertor leg. For the HFS divertor leg, the simulation results in cold and dense plasma conditions, however, without complete detachment as observed in the experiment. Finally, it should be noted that the simulation exhibits a mostly stagnant plasma in the main SOL, in contrast to the experimentally observed parallel flow pattern toward the inner divertor [16].

To simulate gas injection, impurities are launched inside DIVIMP at a specified location on the grid either as atoms or ions. Depending on the number of wall vertices, 10^4 to 10^6 particles are typically launched to obtain sufficient statistics of wall deposition. Atoms are assumed to travel in straight lines from their injection point until they are ionised or hit a wall element. Upon ionisation impurity ions experience friction with the background deuterium plasma, as well as forces due to the parallel electric field

5

and due to temperature gradients along the field line [7]. Impurity ions are also followed as they become ionised to higher charge states or recombine due to electronic recombination and charge exchange with the background plasma.

For the simulation of the gas injection, the ^{13}C source was approximated by direct injection of singly ionised carbon, ^{13}C^{+}. This approach is justified by taking into account that in the halo plasma region the plasma conditions are sufficient to dissociate injected methane (see Ref. [16]). Because the injection valve used in the experiment is located about 10 cm outside of the computational grid it is safe to assume that the injected methane molecules have been fully dissociated and ionised upon grid entry. The transport of the injected ^{13}C is followed until it strikes a main wall or divertor element, where the deposited atoms are accounted for deposition. Re-erosion of deposited ^{13}C was not considered in this work.

For particles leaving the grid in the main chamber, DIVIMP assumes in the simplest approximation that the particles are instantly deposited on the wall segment closest to the current grid boundary cell. This simplification is a consequence of the limitation of the current computational grid as discussed above. The large gap between the radially outermost grid cells and the wall, particularly at the top of the device and below the LFS midplane may lead to artificially large deposition on specific wall segments directly adjacent to the respective exit grid cell, whereas in reality, the particles would be deposited further away from such a cell due to transport processes in the halo plasma region outside the grid. In the course of this work, the DIVIMP code was modified so that the particles are followed for a short period of time after leaving the grid, taking into account their charge state, so as to better approximate where the particles get deposited. However, the lack of plasma background outside the standard grid still limits the accuracy of this method.

3. ^{13}C injection experiments in AUG L-mode plasmas

On the last day of plasma operations of the AUG 2004-2005 experimental campaign, ^{13}CH$_4$ was injected into the torus during a series of identical, lower single-null L-mode discharges (#24046 to #24059). The gas injection was accomplished from a single valve at the low field side midplane, hence, in toroidally asymmetric fashion. Toroidally symmetric ^{13}C deposition may therefore not be necessarily assumed. The experiments were performed in
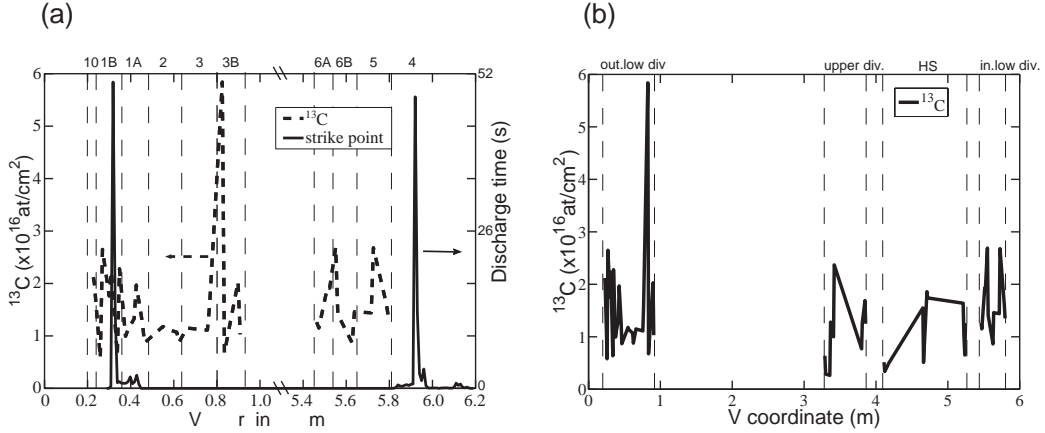
Figure 3: (a) ^{13}C distribution at the lower divertor (dashed line) together with the integrated strike point position residence time from magnetic reconstruction during the last fourteen shots (solid line). The tile numbers shown on top of the plot correspond to the tile numbers given in Fig. 1(a). (b) ^{13}C distribution over the entire chamber. Figures cited from Ref. [11].

hydrogen, and not in deuterium, to decrease activation of the device on the last day of the campaign. Details of the experimental setup, and of ^{13}C deposition measurements and their analysis can be found in Ref. [11]. For the comparison of the DIVIMP simulation with the measured deposition profiles, the main experimental results are summarised in this section.

The deposition profile of ^{13}C along the lower divertor target, together with the residence time histogram of the strike point position during the last fourteen shots of the 2005 campaign, are shown in Fig. 3(a) [11]. The V-coordinate represents the distance from the private flux region along the walls in the counter-clockwise direction, and thus gives the poloidal position. The origin of this coordinate, V = 0 m, corresponds to the top edge of the dome baffle (Fig. 1(a), tile 9A). Starting from V = 0 m, the vessel wall is divided into a number of regions, as follows: the LFS lower divertor, the limiter, the upper divertor, the central column heat shield, the HFS lower divertor, and the dome baffle. During the ^{13}C injection experiments the strike points were at the divertor tile 4 and the LFS divertor tile 1B.

Several ^{13}C peaks are observed on the LFS target plate, tile 1B (V = 0.27, 0.31 and 0.35 m), and the inner divertor tiles, 6B (V = 5.55 m) and 5 (V = 5.73 m) Fig. 3(a). The peaks on the tile 1B are shifted toward the dome baffle, i.e. downward, with respect to the LFS strike point. Unfortunately

7

samples from the inner target plate, tile 4, were not available for analysis. A large peak of ^{13}C was observed on the horizontal LFS divertor baffle, tile 3B (V = 0.83 m). Assuming toroidal symmetry of the deposition, the total amounts of ^{13}C deposited onto the HFS and LFS lower divertor were found to correspond to total amounts of 4.2×10^{20} and 11.1×10^{20} atoms, respectively, which add up to 9% of the total injected amount. On the central column heat shield and upper divertor tiles, total amounts of 6.9×10^{20} and 9.8×10^{20} atoms of ^{13}C were estimated, respectively, from the analysed tiles. These numbers represent 4% and 6% of the total injected amount. The detailed distribution of ^{13}C as a function of the V-coordinate over the entire poloidal cross-section is shown in Fig. 3(b). At the central column heat shield ^{13}C deposition increases from the top towards the middle part and then decreases towards the lower divertor.

To investigate the local deposition of ^{13}C, samples from the limiter tiles located near the puffing valve were analysed. Because samples were available only from the limiter tile close to the valve and from the top tile, as a first approximation, a linear decrease of the ^{13}C deposition along the limiter surface from the middle to the top and to the bottom was assumed. Integrating over the limiter surface, it was found that 4.2×10^{20} atoms, i.e., 2.4% of the puffed amount of ^{13}C, was deposited onto the limiter tiles in the vicinity of the puffing location. Thus, the limiter, the lower and upper divertors, and the heat shield tiles account for 21.0% of the ^{13}C that was puffed into the machine. The deposition results are summarised in Tab. 1. Without further analysis of additional samples, one can only speculate about the deposition location of the remaining 80% of the injected ^{13}C. One source of uncertainty is the extrapolation from local measurements to the entire first wall assuming toroidal symmetry. A significant fraction of ^{13}C might have also be deposited at limiter side faces and inside tile gaps. Furthermore, the generally observed pattern of low-Z impurity deposition at the inner strike zone implies that a part of the missing fraction is due to deposition on tile 4, which could not be retrieved. In addition, one also has take into account that the injection valve is recessed in a midplane port duct. Measurements with a fast reciprocating probe showed the presence of a low-density plasma extending far outside the SOL (see Ref. [16]). Hence, a significant amount of the methane molecules dissociated already inside the port duct and locally re-deposited there. No samples were taken from the port duct.

As the DIVIMP model does not include the aforementioned deposition channels, in the following analysis of the simulations, the deposition results

were normalised to the experimental total amount of 21%.

4. DIVIMP simulation results

4.1. Base case setup

The DIVIMP base case simulation shows that most of the injected ^{13}C is re-deposited at the LFS midplane, in the vicinity of the injection location (Fig. 4). Only a few percent are deposited at the LFS target plate, and an even smaller fraction at the inner target plate. Deposition at the upper divertor and the central column heat shield is negligible. For the base case simulation a ^{13}C point source at the outermost grid cell at the LFS midplane ($d = 4.20$ cm) was assumed. Here, the parameter d is the radial distance from the closest vertex of the wall description. The separatrix is located at $d = 5.13$ cm, i.e., particles injected at $d > 5.13$ cm are introduced in the confined plasma region. For the radial transport, a perpendicular anomalous diffusion coefficient of $D_\perp = 1.0$ m^2/s was assumed.

In the subsequent sections, the sensitivity of the base case results on variation of the cross-field diffusion coefficient for carbon ions and the ionisation and source distribution profiles of the injected carbon are discussed.

4.2. Variation of the cross-field diffusion coefficient

In first approximation a radially constant diffusion coefficient was assumed for the cross-field transport of ^{13}C ions. In the studies conducted by Elder *et al.* [8], the optimal value for the cross-field diffusion coefficient for an L-mode shot at DIII-D was found to be $D_\perp = 0.4$ m^2/s. The effect of the cross-field diffusion on the ^{13}C deposition in the case discussed here was studied by varying the value of $D_\perp$ over a full order of magnitude, $D_\perp = 0.5$ m^2/s – 5.0 m^2/s. Increased $D_\perp$ resulted in an increased re-deposition at the LFS limiter, while the change in $D_\perp$ had no dramatic effects on the deposition pattern on the divertor or the central column heat shield. The increase of local re-deposition around the injection valve location with increasing value of $D_\perp$ is an obvious consequence of increased perpendicular flux at unaltered parallel transport. Unfortunately, detailed experimental measurements on the limiter surfaces do not exist and, thus, no direct conclusive result for the actual value of $D_\perp$ cannot be derived. Hence, for subsequent simulations an ad-hoc value of $D_\perp = 1.0$ m^2/s was used.

4.3. Variation of the ionisation distance and ionisation source profile

To estimate the influence of the actual ionisation distribution source location of $^{13}C^+$ on the deposition distribution, the distance of the injection location to the wall and the shape of the source distribution was systematically varied. Simulations of the break-up of hydrocarbon molecules using a newly developed DIVIMP module [9], and similar 3D ERO simulations [17] show that the first ionisation of carbon takes place much closer to the vessel wall than the outermost grid cell. As the $^{13}CH_4$ enters the device, it starts experiencing ionisations as well as dissociations due to the high temperature. The most common dissociation processes result in neutral carbon that penetrates further in the device before ionising. To study this behaviour, ideally the recently implemented hydrocarbon breakup model [10] would be employed, but was not done within the scope of this work. Instead, several simulations were performed using the simplifying approximation of launching carbon ions at discrete points of different depths d.

When ^{13}C ions are injected in the SOL as a point source, a large proportion of the injected carbon ions is deposited in the immediate vicinity of the puffing location at the limiter (Fig. 4: $V = 1.5$ m $- = 2.25$ m). This supports the hypothesis that a large portion of the missing ^{13}C fraction in the tile analysis can be attributed to local re-deposition in the gas valve port duct. Significantly less carbon is deposited at the limiter when the injection location is shifted inside the separatrix. Besides the LFS limiter area, the region most sensitive to the wall distance is the inner divertor, where the deposition steadily increases as the distance from the wall is increased. Because the calculated background plasma was stagnant, and no parallel-B flows from the LFS midplane region toward the HFS divertor were assumed in DIVIMP, the most likely route for ^{13}C to enter the inner divertor region is via the confined plasma region. Furthermore, the deposition at the LFS lower divertor becomes narrower and shifts toward decreasing V as the injection depth is increased.

Assuming more realistic ionisation source distributions over the delta-function point source distribution, further simulations were carried out using a radial source distribution with a suitable envelope function. Two different envelope functions were used: a rapidly decaying Gaussian $\exp(-(d-\mu)^2/\sigma^2)$, where μ is the horizontal distance of the peak of the Gaussian from the wall and σ the width of the envelope, and a more slowly decaying exponential function, $\exp(-(d-\mu)/w)$, where w now stands for the decay length and μ
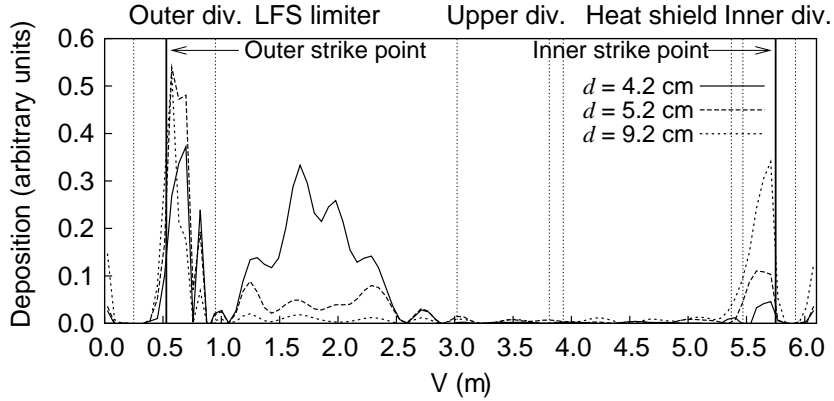
Figure 4: Deposition profiles produced using different depths, d, for the point source. The location of the point source is found to dramatically affect the relative strength of the in/out asymmetry of the divertor deposition as well as the deposition on the low field side (LFS) limiter.

is the horizontal distance of the maximum from the wall, i.e. the starting point of the profile.

Assuming Gaussian profiles for the injection of ^{13}C, the calculated ^{13}C deposition profiles for various injection locations are qualitatively the same as the corresponding cases assuming a point source Fig. 5. Here, a source width of 3.2 cm was assumed for all Gaussian injection profiles.

Assuming an exponentially decaying distribution as suggested by results of ERO simulations [17] does not significantly change the calculated ^{13}C deposition pattern in the divertor regions compared to those for the point source and Gaussian source distributions (Fig. 6). The differences between the three tested injection depth profiles are less pronounced as compared to the other source options. Here, the decay length of the exponential function was chosen to $w = 5$ cm, which is larger than the values suggested by the ERO simulations, but results in a better agreement with the measurements. Larger decay length corresponds to assuming higher fraction of ions penetrating deeper into the SOL. As observed for the other distribution functions, the source profile peaking at 4.0 cm displays an increased deposition in the LFS limiter region, which unfortunately was experimentally inaccessible. Similar to the trend for the other source options, as the peak of the source profile is moved towards the separatrix, this deposition is reduced, deposition on the inner divertor is increased, and the deposition profile in the LFS lower
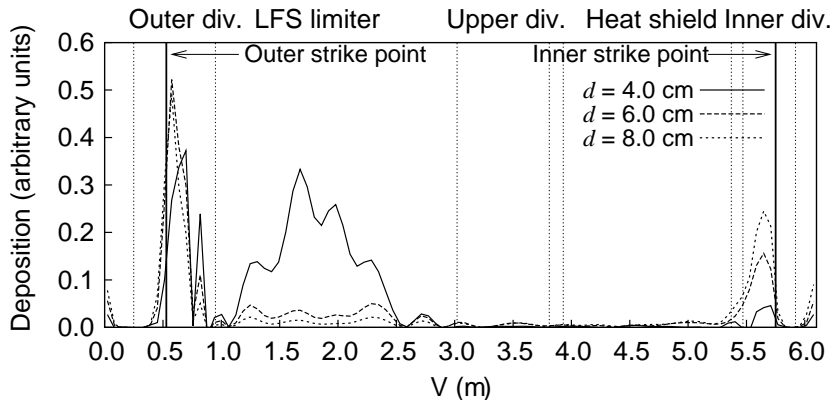
11

Figure 5: Deposition profile resulting from Gaussian ionisation source profiles of fixed width centered at different depths, d.

divertor becomes narrower.

5. Discussion and Conclusions

Carbon migration and deposition in ASDEX Upgrade $^{13}CH_4$ puffing experiments were simulated using the Monte-Carlo based impurity transport code DIVIMP. The simulated wall deposition profiles were compared to experimental results obtained by post mortem SIMS analysis.

While the general pattern of the measured deposition profiles could be replicated by the simulations, particularly in the divertor region, quantitative agreement between the modelled results and the experimental observations could not be tested because of the lack of deposition measurements for the inner divertor (tile 4). The comparison of the measured and predicted deposition profiles is hampered by the fact that only 21% of the injected ^{13}C was found inside the vacuum vessel. This may be due to the toroidally localized injection itself, potentially leading to toroidally asymmetric ^{13}C deposition in the divertor. The injection itself may also have disturbed the local plasma parameters at the low field side midplane region. Furthermore, no deposition measurements were made at the divertor dome. As observed in the case of DIII-D, the surface facing the divertor private flux region can be regions of strong ^{13}C deposition [18]. Until these measurements are made, through new experiments, the interpretation of the results with regard to both the experiments and simulations remain questionable.
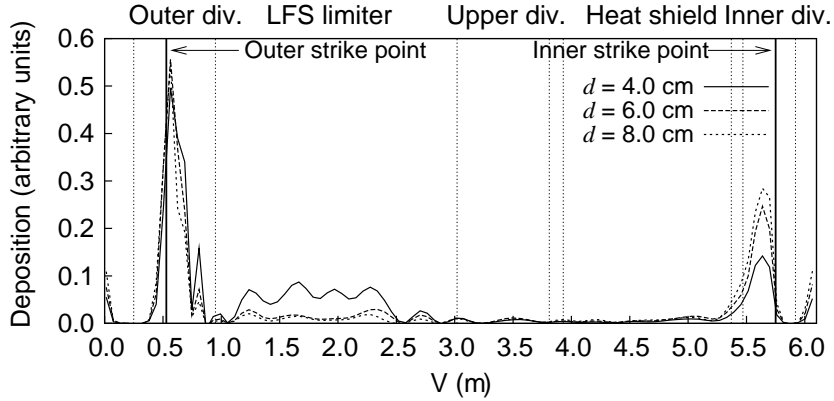
Figure 6: Deposition profile resulting from decaying exponential ionisation source profiles of fixed width centered at different depths, d.

Table 1: Carbon deposition on the various sections of the vessel wall obtained from the measurements and by simulation using a Gaussian ionisation source profile. The simulated ^{13}C deposition was normalized to the total amount of ^{13}C measured. A perpendicular diffusion coefficient of 1.0 m^2/s was used.

	Simulation	Measurements
HFS lower divertor	4.4%	2.4%
LFS lower divertor	11%	6.5%
Upper divertor	0.6%	4.0%
Heat shield	0.01%	5.7%
LFS Limiter	4.4%	2.4%

The simulations reproduced the overall deposition at the LFS strike zone, $\mathsf{V} = 0.25 - 0.5$ m, consistent with the measurements (Fig. 3(a)). However, the prominent peak in the experimental deposition profile, located on the tile 3B at around $\mathsf{V} = 0.8$ m cannot be replicated with the present simulations, likely because of the computational grid not extending to the wall. Already at the injection location at the LFS midplane, there is an approximately 4 cm gap between the outermost grid cell and the wall. As discussed in Sec. 3, the injected methane is likely to dissociate outside the grid and, consequently, methane radials and ^{13}C$^+$ ions start moving in the direction of the magnetic field lines before even reaching the region covered by the grid. As a result, such ions will partly be transported along the field lines intersecting the

13

horizontal part of the vessel wall, where the largest deposition was measured. In the simulations strong ^{13}C deposition at the LFS limiter was also observed in the vicinity of the gas injection valve, consistent with the measurement.

Significant uncertainty in the simulations is introduced by prescribing the cross-field diffusion of ^{13}C ions and the ionisation source profile. A scan of the cross-field diffusion coefficient reveal that the overall ^{13}C re-deposition pattern away from the injection location is insensitive to the changes in $D_\perp$; only the region directly adjacent to the injection location is affect by the magnitude of $D_\perp$. A much larger effect on the divertor deposition was observed for the variation of the radial source location. With deeper sources, the deposition fraction at the inner divertor target plate increased due to increased migration through the confined plasma region. Changes of the radial width and shape of the source distribution resulted in small variations of this general observation. The closest agreement between the measured and simulated deposition profiles were obtained when assuming a perpendicular diffusion coefficient of $D_\perp = 1.0$ m^2/s and a Gaussian source distribution centered in the core plasma, $d = 6.5$ cm, and with standard deviation of $\sigma = 3.2$ cm (Tab. 1). The significantly smaller deposition calculated at the central column heat shield compared to the experimental results indicates that apart from the issues of having a large gap between the computational grid and the wall, the model also suffers from the lack of parallel flows in the main SOL, which were measured in many tokamaks. These flows have yet not been reproduced reliably in fluid code simulations. Further studies with more sophisticated codes are required to improve our understanding of the relevant transport processes.

Acknowledgments

References

[1] G. Federici, R. A. Anderl, P. Andrew, J. N. Brooks, R. A. Causey, J. P. Coad, D. Cowgill, R. P. Doerner, A. A. Haasz, G. Janeschitz, W. Jacob, G. R. Longhurst, R. Nygren, A. Peacock, M. A. Pick, V. Philipps, J. Roth, C. H. Skinner, W. R. Wampler, Journal of Nuclear Materials 266-269 (1999) 14–29.

[2] G. Federici, P. Andrew, P. Barabaschi, J. Brooks, R. Doerner, A. Geier, A. Herrmann, K. Krieger, A. Kukushkin, A. Loarte, R. Neu, G. Saibene, M. Shimada, G. Strohmayer, M. Sugihara, Journal of Nuclear Materials 313-316 (2003) 11.

[3] J. Likonen, S. Lehto, J. Coad, T. Renvall, T. A. T. Sajavaara, D. Hole, G. Matthews, J. Keinonen, C. to the EFDA-JET work programme, Fusion Engineering and Design 66-68 (2003) 219–224.

[4] E. Vainonen-Ahlgren, J. Likonen, T. Renvall, V. Rohde, R. Neu, M. Mayer, R. Pugno, , K. Krieger, A. U. Team, Journal of Nuclear Materials 337-339 (2005) 55–59.

[5] S. Allen, W. Wampler, A. Mclean, D. Whyte, W. West, P. Stangeby, N. Brooks, D. Rudakov, V. Phillips, M. Rubel, G. Matthews, A. Nagy, R. Ellis, A. Bozek, Journal of Nuclear Materials 337-339 (2005) 30–34.

[6] D. Naujoks, R. Behrisch, J. Coad, L. de Kock, Nuclear Fusion 33 (1993) 581.

[7] P. Stangeby, C. Farrell, S. Hoskins, L. Wood, Nuclear Fusion 28 (11) (1988) 1945–1962.

[8] J. Elder, P. Stangeby, D. Whyte, S. Allen, A. McLean, J. Boedo, B. Bray, N. Brooks, M. Fenstermacher, M. Groth, C. Lasnier, S. Lisgo, D. Rudakov, W. Wampler, J. Watkins, W. West, Journal of Nuclear Materials 337-339 (2005) 79–83.

[9] A. McLean, J. Elder, P. Stangeby, S. Allen, J. Boedo, N. Brooks, M. Fenstermacher, M. Groth, S. Lisgo, A. Nagy, D. Rudakov, W. Wampler, J. Watkins, W. West, D. Whyte, Journal of Nuclear Materials 337-339 (2005) 124–128.

[10] J. Elder, A. McLean, P. Stangeby, S. Allen, J. Boedo, B. Bray, N. Brooks, M. Fenstermacher, M. Groth, A. Leonard, D. Rudakov, W. Wampler, J. Watkins, W. West, D. Whyte, Journal of Nuclear Materials 390-391 (2009) 376–379.

[11] E. Vainonen-Ahlgren, J. Likonen, T. Renvall, V. Rohde, M. Mayer, A. U. Team, Journal of Nuclear Materials 363-365 (2007) 270–275.

[12] P. Stangeby, J. Elder, J. Boedo, B. Bray, N. Brooks, M. Fenstermacher, M. Groth, R. Isler, L. Lao, S. Lisgo, G. Porter, D. Reiter, D. Rudakov, J. Watkins, W. West, D. Whyte, Journal of Nuclear Materials 313-316 (2003) 883–887.

[13] P. Stangeby, J. Elder, Nuclear Fusion 35 (1995) 1391–1412.

[14] R. Schneider, D. Reiter, H. Zehrfeld, B. Braams, M. Baelmans, J. Geiger, H. Kastelewicz, J. Neuhauser, R. Wunderlich, Journal of Nuclear Materials 196-198 (1992) 810–815.

[15] D. Reiter, Journal of Nuclear Materials 196-198 (1992) 80–89.

[16] H. Muller, V. Bobkov, A. Herrmann, M. Maraschek, J. Neuhauser, V. Rohde, A. Schmid, M. Tsalas, A. U. Team, Journal of Nuclear Materials 363-365 (2007) 605–610.

[17] P. Kall, 3d simulations of impurity transport in the divertor region of asdex upgrade tokamak, Master's thesis, Helsinki University of Technology (2005).

[18] W. Wampler, A. McLean, S. Allen, N. Brooks, J. Elder, M. Fenstermacher, M. Groth, P. Stangeby, W. West, D. Whyte, Journal of Nuclear Materials 363-365 (2007) 72–77.